The Effects of Slider Design on Thermal Asperity Rejection Capability

Vinod Sharma, Seong-Hoon Kim, Sung-Hoon Choa*†
Samsung Information System America, San Jose, CA 95134, USA

Particle contamination has been an ongoing problem affecting the reliability of the magnetic hard disk drives. Especially the recent use of MR head requires much tighter control of particle contamination due to thermal asperity (TA) phenomenon. In this study, the effects of slider air bearing surface design on TA reduction capability were investigated by manufacturing two types of sliders. Numerical methods were used to simulate the motion of particles in the head/media interface. Experiments were conducted to verify the results predicted by the numerical simulation. Drives were built and exposed to particle contamination using a particle injection chamber, which turned out to be a very simple and reliable particle generation method over conventional aerosol technique. Then the number of TA generated in the drives was recorded and compared. Also the contacts between slider and particles were investigated by acoustic emission study. It was found that a new ABS design, which has aerodynamic U-shaped rail and central flow passage, was beneficial in reducing the particle contamination on the slider.

Key Words : Hard Disk Drive(HDD), Thermal Asperity, Acoustic Emission

1. Introduction

In magnetic hard disk drives, particle contamination has been an important factor which influences the reliability of the drive. Particle-induced damage on the disk and head surface not only causes localized data losses but can lead to catastrophic head crashes. Particle-induced damage generally results from particle buildup on the slider and embedding of the particles on the disk (Koka, 1989; Hiller and Brown, 1992). Hiller et al. (1994) proposed that particles entering the head/media interface can be accumulated at the trailing edge of the slider through whisker formation mechanism. They found that the continuous process of breaking-off and redeposition of the whiskers on the slider could lead to a loss of air bearing pressure and head crash. Altshuler et al. (1998) and Zhang et al. (1999) extensively studied the level of physical damage caused by particle contamination. They found that the severity of physical damage to head/disk interface is dependent on the hardness and ductility/brittleness of the particle. Therefore, harder particles cause more physical damage. Particle shape and size can also be contribution factors in damaging the head/disk interface.

With the use of magneto-resistive (MR) heads in drives, particle contamination has resurfaced as an important factor affecting drive reliability and manufacturing yield. Heating of MR sensor due to the contact with particle contamination will cause distortion of output signal, which is generally defined as a thermal asperity (TA) (Klaassen and van Peppen, 1997; Sawatzky, 1998). During the read/write process, occurrence of a significantly large TA can lead to an unrecoverable read error, resulting in the failure of the drives. Consequently, the drives using MR head became much more sensitive to particle contami-

† First Author
* Corresponding Author,
E-mail : shchoa@sisa.samsung.com
TEL : +82-31-200-4749 ; **FAX** : +82-31-200-3144
Samsung Information System America, San Jose, CA 95134, USA. (Manuscript **Received** October 16, 1999; **Revised** December 14, 2000)

nation. Over the past years, considerable efforts have been spent to eliminate TA. Since TA generally results from loose particles such as dust or other debris from drive components or manufacturing process, main effort has been focused on much tighter control of cleanliness of the drive components and manufacturing process. However, there are little studies on the effect of head and disk design on TA reduction. Recently, Zhang et al. (1997) proposed an idea that optimization of slider air bearing surface (ABS) design can reduce TA by guiding the particles away from the MR sensor, which is located on the trailing edge of the slider. They claimed that the reduction of TA or particle contamination can be possible by modification of ABS design, which prevents the particles from moving through the trailing edge. In other words, the idea is to make the particles move out of the air bearing surface from the two sides as easily as possible. Using numerical simulation, they analyzed the paths of particles moving in the air bearing for various designs of sliders, and found that some slider designs have beneficial effect on reducing the particle contamination on the slider.

In this study, we extended their work by performing particle experiments, and further proposed another strategy of slider ABS design to reduce TA. A numerical method was used to simulate the motion of particles in the head/media interface for two types of sliders. Then, experiments were conducted to verify the results predicted by the numerical simulation. Drives were built with two types of sliders and exposed to particle contamination. For precise control of particle generation and counting, a particle injection chamber was made. Then the number of TA generated in the drive due to particle contamination was compared for the two sliders. Also the contact between the slider and particles was investigated by acoustic emission (AE) study.

2. Numerical Analysis

Since large amounts of particles that cause contamination are brought into the head/media interface by air flow, it is important to understand

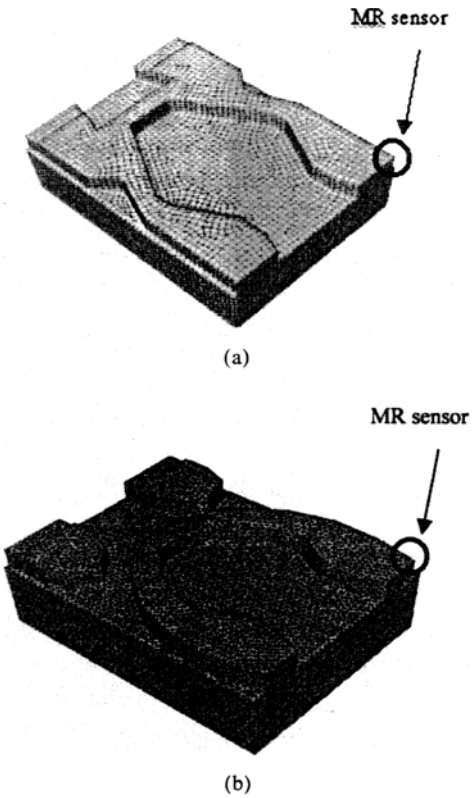

Fig. 1 Air-bearing-surface (ABS) shape of (a) type A slider, (b) type B slider

how these particles move in the head/media interface. Therefore, the purpose of computer simulation in this study is to find how particles move through the air bearing surface and leave the slider from the trailing edge. In addition, from particle path visualization, we can obtain physical insight to design better ABS for reducing particle deposition near the MR sensor. Figure 1 shows the ABS model of two different types of the slider used in the computer simulation, which are noted as Type A and Type B. Figure 2 also shows the detailed geometrical shape and dimensions for each head. The MR sensor of both sliders is located at the end of the trailing edge area. Type A slider is a conventional negative pressure ABS design, which has a tapered leading edge and a recessed cavity between two rails to provide negative pressure. Type B slider is the modified version of type A designed to reduce the particle contamination on the slider. A characteristic of type B slider is that it has a U-shaped (or wedge-

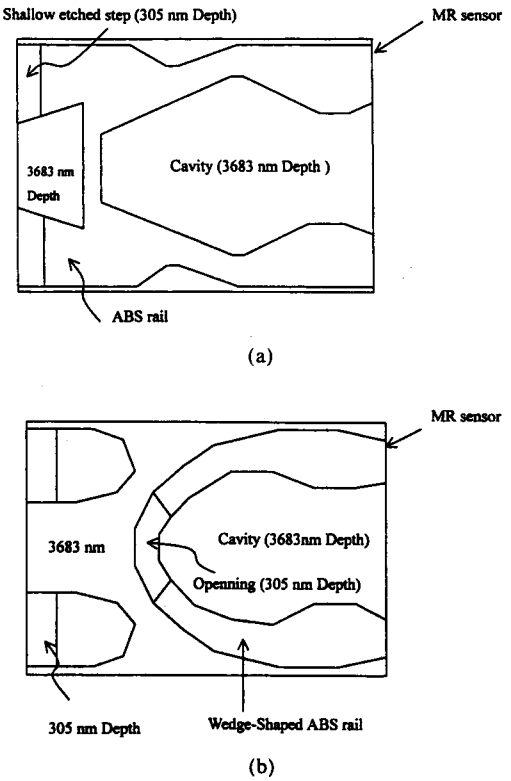

Fig. 2 Geometrical shape of Air-bearing-surface (ABS) shape of (a) type A slider, (b) type B slider

shaped) channels in the leading edge to tailor the flow of particles away from the MR sensor. Also it has an opening in the center part of the U-shaped channel that helps to guide the particles away from the MR sensor.

The governing equations that are considered for particle tracing are general steady three-dimensional Navier-Stokes formulas, since fine particle traces are similar to streamlines of air flow. The equations are:

$$\nabla \cdot \mathbf{u} = 0 \tag{1}$$

$$\rho(\mathbf{u} \cdot \nabla)\mathbf{u} = -\nabla p + \mu \nabla^2 \mathbf{u} + \mathbf{f} \tag{2}$$

where $\mathbf{u}$ is the velocity component, ρ is the density of air, p is the pressure, μ the is viscosity of air, and $\mathbf{f}$ is the body force that includes gravity force. Here we do not consider particle transport separately. In addition, we do not include the effect of compressibility of air flow since our current study is only focused on the motion of

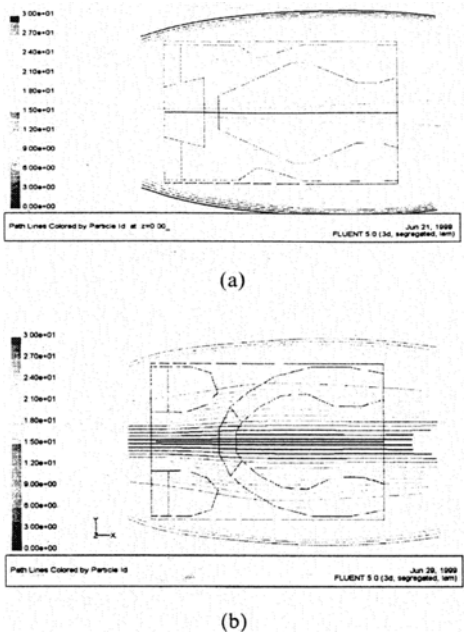

Fig. 3 Particle traces released at surface of rail for (a) type A slider (b) type B slider

particle in head/media interface and the compressibility effect does not affect on the trend of air flow motion.

For the boundary conditions, the input velocity is the same as the disk rotating speed along the z direction (rail height) because the height of the physical domain is so small that we could assume same velocity at the entrance region without loss of physical meaning. As an evidence the boundary layer thickness near 3.5 inch disk is around 0. 5 mm for 5400 rpm operation. These governing equations and boundary conditions are solved by Fluent 5.0 that uses finite volume method. The geometric modeling and mesh generation are carried out through Gambit 1.0 that was originally developed by FIDAP.

The physical domain of flow field for ABS is shown in Fig. 3. In order to figure out the role of slider rail, we magnify the scale in z direction by 50 times. By comparing type A with type B, we can notice that type A has long and straight rails that increase the possibility of particle embedding under both side rails. Figure 4 depicts the particle traces for each type of ABS when particles release at the bottom of the rail.

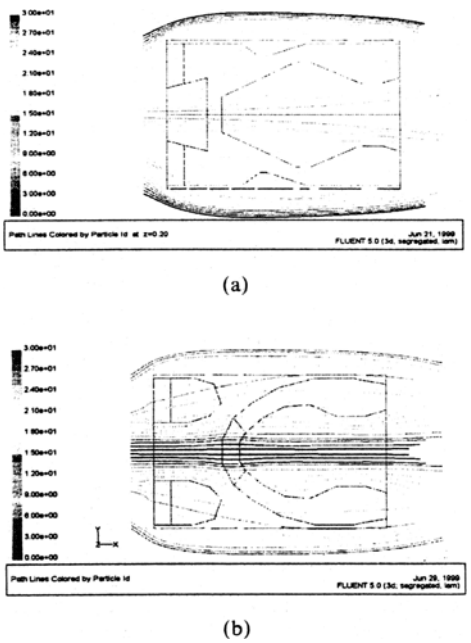

(a)

(b)

Fig. 4 Particle traces released at bottom of slider rail for (a) type A slider (b) type B slider

While a lot of particles pass through the MR sensor zone in type A, fewer particles pass through that area in type B. Thus the design of type B has some advantages over that of type A for two reasons. First, the aerodynamic U-shaped rail decreases the possibility of particle deposition. Second, the central flow passage prohibits particles from embedding under the side rails and protects the transducer from outside airflow.

3. Experimental Procedure

3.1 Head and disk

This work includes two sets of experiments. The first experiment involves drive level particle injection test and the second experiment involves disk component level test. Two types of sliders were manufactured as shown in Fig. 5 on the basis of the numerical models. In manufacturing the type B slider, the taper leading edge of the slider was slightly modified to compensate the effects of the skew angle, which refers to the angle between slider's longitudinal direction and the air flow direction during seeking operation of the head. Except for the ABS slider design, all characteristics of both heads including electrical performance and flying height were identical.

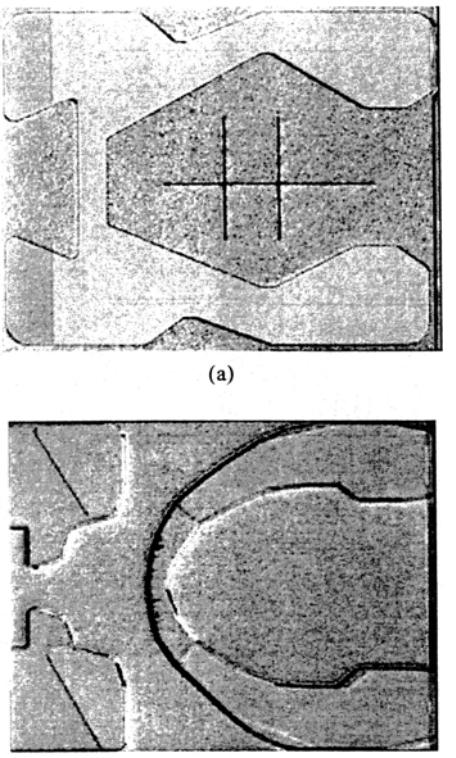

(a)

(b)

Fig. 5 ABS surfaces of both heads (a) type A head (b) type B head

Both heads are 50 percent nano sliders with MR element. They are made from Al_2O_3-TiC, and have a nominal flying height of 40 nm (1.6 μ in) at an operation speed of 5400 rpm. The MR sensor has a writer width of 2.5 μm and reader width of 2.0 μm with a resistance of 35 ohms. Figure 6 is a schematic drawing of the side profile for tested head when it is flying over a disk at the operating speed. The steep slope at the front end represents the leading edge taper, through which air gets into the air bearing surface. The leading edge taper is the largest opening between a slider and a disk. The front and back end of the taper is 4 μm and 3.7 μm from the disk surface. The gentle slope after the leading edge taper is part of the ABS which is made of two rails. At the trailing end of the slider is a short section of sputtered alumina in which MR sensor is encapsulated.

The disk used in the test was a laser textured 95 mm diameter AlMg/NiP substrate. The disk is overcoated with nitrogenated carbon, about 100 Å thick, and lubricated with 14 Å of perfluoropolyether (PFPE) type lubricant. The surface roughness of the data zone is 5. 5 Å Ra.

3.2 Drive level particle injection test

In this study, alumina (Al_2O_3) powder was used as particle contaminants, which has a normal distribution with a mean diameter of 1 μm. Alumina particle was chosen because it was commonly used in the manufacturing of disk drive component as a slider material and a disk texturing slurry. In reality, alumina particle was found to be the typical source of thermal asperity in the drive (Zhang, 1999). One-micron size was also chosen because most of the observed TAs in our drives were in this range. Several studies showed

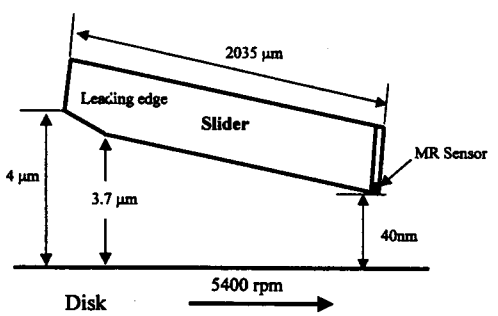

Fig. 6 Interface profile when a slider flies over a disk

the way of introducing particles in a hard disk drive using aerosol technique (Bergin and Koka, 1992). However, this technique requires expensive and sophisticated test set-up as well as tedious work. In this study, particles were introduced into a hard disk drive using a particle injection chamber. We found that this technique is very simple and repeatable, and can be used as a substitute for conventional aerosol technique.

The schematic diagram of the particle injection chamber is shown in Figure 7. A chamber was built to generate a uniform environment around the drives. The chamber consists of three sub-chambers. The sub-chamber on the left has two fans and a deflector. Particles are introduced in this sub-chamber and they circulate in the left and middle sub-chambers. A shutter separates the middle sub-chamber from the right sub-chamber and helps to control the concentration of particles. Drives are placed in the right sub-chamber. The drives may be directly or indirectly exposed to external environment depending on the type of tests. The concentration of particles can be monitored on-line using a laser particle counter (LPC) connected to the middle sub-chamber. A Met One laser particle counter was used for counting the particles. The flow rate for this particle counter was 0.017 m^3/min. When the shutter is opened, drives are exposed to the particles. The number of particles deposited can be maintained at a relatively constant level by adjust-

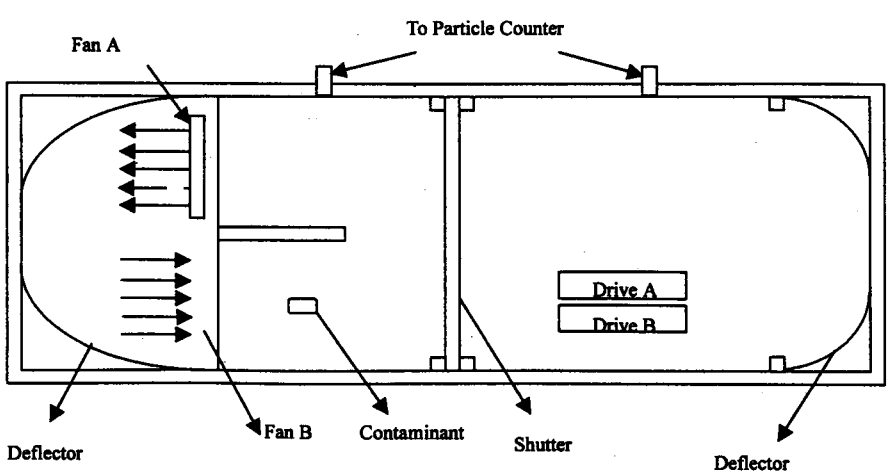

Fig. 7 Schematic configuration of particle injection chamber

ing the time that the shutter is open and by knowing the total number of contaminants in the chamber. The clock port of the drives is opened and the drives are exposed to the particles for one minute. The air flow pattern in front of the drives is very uniform so that two drives can be tested at the same time for comparison. After the drives were exposed to the particles, drives were subjected to a specific test sequence which was design to record any TA events in the drive. Thus, the total number of particles was monitored for each test. The drives were then exposed again to the particles and the number of TA was monitored for all heads and disk surfaces. This process was continued 10 times. If the total number of detected TA reached close to 255 (maximum TA allowed) the drive would turn itself off.

3.3 Component level test

In this study, acoustic emission was used to identify contact between the particle and head when the head flies over the disk. Acoustic emission has been widely used to detect contacts between head and disk (McMillan et al., 1995; McMillan and Talke, 1998). The contact between head and disk was determined by measurement of slider ringing mode in the frequency domain. Here, acoustic emission was used to detect contacts between the head and particle or contaminants on the disk. Since the slider-disk or slider-particle contacts excite the resonance frequencies of the slider, it is apparent that AE signal contains detailed information concerning slider-particle contacts. TTI CSS tester was used as a spin stand tester to obtain AE signal. A differential AE sensor (Micro-100D) was mounted on the slider arm of TTI tester. The AE signal is triggered and captured only when it exceeds a certain threshold. By using a digital oscilloscope, the captured transient AE signal is converted into frequency domain to observe the slider ringing mode which indicates the contact between the slider and particles on the disk. Each spectrum is averaged when AE event occurs above the threshold.

Particles were introduced onto the disk surface with a clean cotton swab. A cotton swab was dipped into a reservoir of particles and then particles were carefully sprayed on a fresh disk surface from a cotton swab. This simple technique offered reasonable control over quantity and location of the particles

Table 1 Number of TAs observed during the first set of the test for type A and type B slider drives, and number of particle measured in particle injection chamber

No.of Test	No of TA	No of TA	Number of different size particles measured with particle counter					
	type A ABS	type B ABS	0.2-0.3 μm	0.3-0.5 μm	0.5-1.0 μm	1.0-3.0 μm	3.0-5.0 μm	>5.0 μm
1	**38**	45	1605	543	8032	7039	2255	0
2	**117**	43	1618	690	8604	8422	2443	0
3	**100**	50	0	406	10051	8338	2578	0
4	**152**	50	1590	721	11359	9665	2950	1
5	**125**	55	1692	797	10006	8268	2603	0
6	**127**	56	1316	377	6164	5201	1402	0
7	**111**	126	1666	688	10971	9398	2798	0
8	**124**	134	1397	721	7600	6865	1957	0
9	**121**	128	944	1299	17347	14122	3845	0
10	**142**	141	0	1475	20652	21398	6862	2

4. Results

4.1 Drive level particle injection test

Drives were built with both types of ABS as shown in Fig. 5. The both drives were put into the particle injection chamber in parallel and exposed to the particles. After exposure to the particles, the number of TA was scanned for each drive. Tables 1~3 show the results from the three different sets of tests performed on both types of slider. Table 1 shows the results of the number of TA generated in the drives as well as the number of different size particles in the chamber measured by the laser particle counter. Particle counter measurement indicated that the size of the alumina particle ranged from 0.2 μm to 5 μm. However, the dominant size of the particle was from 0.5 μm to 3 μm. As shown in Table 1, type A slider generated more TA than did type B up to the sixth repeated test. After that, type A produced the similar number of TA compared with type B. For the second drive test as shown in Table 2, however, the number of TA for type A

Table 2 Number of TAs observed during the second set of the test for type A and type B slider drives, and number of particle measured in particle injection chamber

No.of Test	No of TA	No of TA	Number of different size particles measured in Particle Counter					
	type A ABS	type B ABS	0.2-0.3 μm	0.3-0.5 μm	0.5-1.0 μm	1.0-3.0 μm	3.0-5.0 μm	>5.0 μm
1	**74**	10	1290	709	12375	11009	3362	1
2	**78**	18	1303	981	11459	9574	2573	
3	**95**	24	1183	936	15898	14252	4677	0
4	**148**	34	1299	1077	15165	14589	4580	0
5	**148**	38	1483	737	11492	10630	3195	0
6	**142**	38	1458	369	7101	6786	2220	1
7	**137**	43	1212	837	16340	14558	4599	1
8	**204**	49	0	1013	21207	19573	6233	0

Table 3 Number of TAs observed during the third set of the test for type A and type B slider drives, and number of particle measured in particle injection chamber

No.of Test	No of TA	No of TA	Number of different size particles measured in Particle Counter					
	type A ABS	type B ABS	0.2-0.3 μm	0.3-0.5 μm	0.5-1.0 μm	1.0-3.0 μm	3.0-5.0 μm	>5.0 μm
1	**8**	7	1464	986	14190	12247	3413	0
2	**11**	11	1427	1200	14749	13102	3825	0
3	**16**	11	1261	889	13858	12894	4019	0
4	**27**	23	1176	1072	15489	13183	3945	0
5	**24**	28	1645	844	11954	10794	3004	0
6	**29**	29	1414	767	9544	8687	2569	0
7	**43**	39	1167	1138	14181	14117	4061	0
8	**44**	40	1505	803	10616	9698	2802	1
9	**51**	39	1309	1021	12809	12207	3878	0
10	**52**	38	1441	590	9578	8573	2950	0

ABS drive is about 4 times as many as that for the type B ABS drive. The third drive test in Table 3 also showed that type A slider produced more TA than type B. Thus it can be concluded that the type B ABS has an advantage in terms of TA rejection over type A ABS. It is consistent with the result shown in Fig. 3 and Fig. 4, implying the effects of ABS shape on particle reduction and subsequently on thermal asperity reduction.

4.2 Component level test

As a component level test, the acoustic emission was used to identify the contacts between the head and the particles on the disk. Thousands of particles were dropped on the fresh disk using a cotton swab. The acoustic emission data was collected by spinning the disk at 5400 rpm for three conditions: (a) with no particle and disk spinning with head flying in the data zone of 29. 21 cm radius (background), (b) dropping the particles at the leading edge of the slider and collect AE scan when the head flies over only on track of the disk (track following operation), (c) same as (b) but head flying over the disk data zone with sweeping action (seeking operation). Figure 8(a) shows the AE spectrum in frequency domain for the background (disk spinning, but head did not fly over the disk) with 400-1000 kHz filter. Figure 8(b) shows the AE spectra for type A heads with track following operation. Two peaks at 720 and 890 kHz are observed. These peaks correspond to the first and second

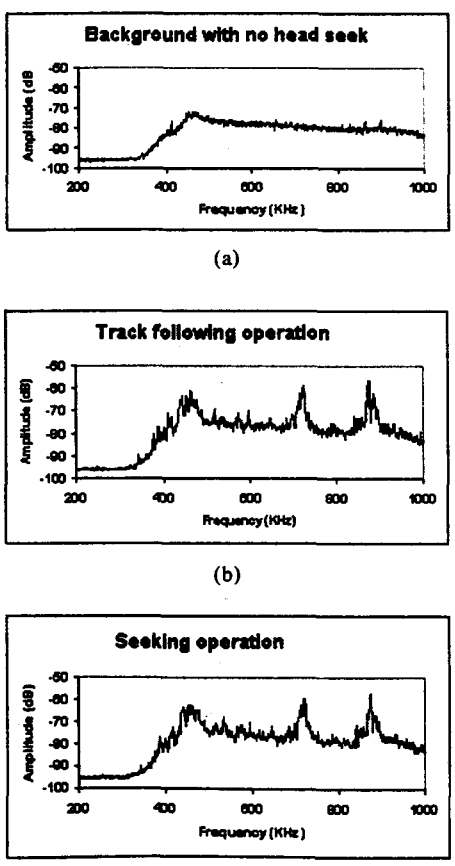

Fig. 8 Typical frequency response of AE signal obtained for (a) no head seek (background), (b) track following, (c) seeking operation for type A head

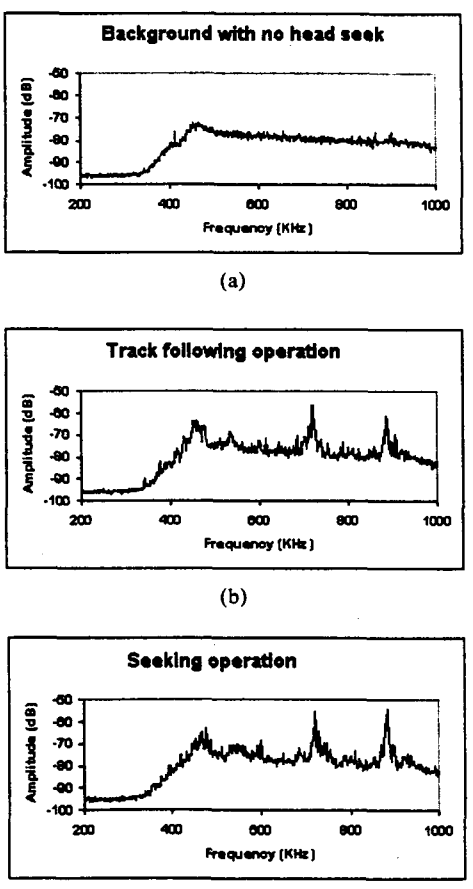

Fig. 9 Typical frequency dependent AE signal obtained, after dropping particles (a) no head seek (background), (b) track following, (c) seeking operation for type B head

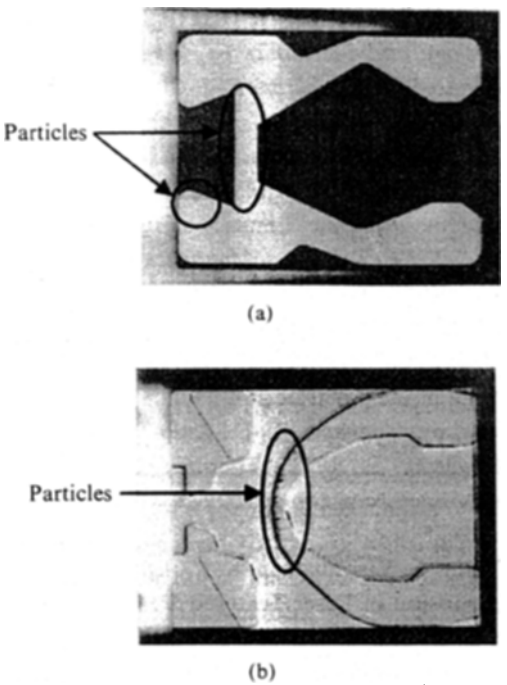

Fig. 10 Typical ABS surfaces after particle test for (a) type A head, (b) type B head

resonance modes of the 50 % nano slider body vibration respectively, indicating that the slider hits the particles during flying (Wang et al., 1998). Figure 9 shows the background AE signal as well as AE signal observed during the track following operation for type B heads. Again, peaks at 720 and 890 kHz are observed. For seek operation of the head in the data zone, these peaks remain unchanged as shown in Fig. 8(c) and Fig. 9(c). In summary, no difference in AE signal was observed for the two type of heads, implying that both sliders are contacting with particles during flying. After the experiment, the heads were observed under an optical microscope. Generally, not many deposited particles were observed on the ABS area. However, for type A head, particles were observed mainly on the straight ABS rail area as shown in Fig. 10(a), on the other hand, for type B head, particles were observed mainly on the opening area of ABS and cavity of the slider (circled regions in Fig. 10(b)). Since a small particle can generate TA when it hits the MR sensor, the location and amount, in which the particle was attached on the slider, are important. From this figure, it appears that particles do seem to get deflected for type B heads compared to type A heads.

Additional tests were performed with much bigger particle, which is 10 μm size glass (SiO_2) particle. Glass particle was used instead of alumina particle since it had very uniform size distribution. For this case, no peaks in the AE signal were observed (not presented in the paper) for track following operation and seek operation. This suggests that 10-micron glass particle was swept away by the slider since they can not enter into the taper leading edge area of the slider. As shown in Fig. 6, 10 μm glass particle is much bigger than the height of leading edge of the slider. For the particles less than the height of the leading edge, they can enter the taper area. Once they go beyond the taper area, the slider ABS rails start contacting with the particles. Subsequently the contacts created the excitation of the slider, which was seen as two peaks in AE signal. Those particles are more likely to generate TA.

5. Conclusions

Two types of heads with different ABS designs were studied for their effectiveness on reducing thermal asperity. Numerical simulation was used to investigate the particle movement through the air bearing surface. In the experimental study, a particle injection chamber was built to inject the particles on the drives instead of using a conventional aerosol technique. This particle injection method turned out to be very simple and reliable. Through numerical and experimental works, it was found that a new ABS design which has aerodynamic U-shaped rail and central flow passage was effective in reducing thermal asperity by guiding the particles away from the MR sensor. The acoustic emission was also used to study the contacts between the slider and particles. For 10-micron glass particles, which are bigger than the height of the slider leading edge, they were swept away by the slider since they can not enter into the taper leading edge area of the slider. For the particles less than the height of the leading edge, they can enter the taper area. Once they go

beyond the taper area, the slider ABS rails start contacting with the particles. Subsequently the contact generates the excitation of the slider. Those particles are more likely to generate TA.

References

Altshuler, K. J., Harrison, J. C. and Ackerman, E., 1998, "The Physical Effects of Intra-Drive Particulate Contamination on the Head-Disk Interface in Magnetic Hard Disk Drives," *ASME Journal of Tribology*, 98-TRIB-47.

Bergin, M. and Koka, R., 1992, "Measurement of Particulate Contamination Levels in Disk Drives with Aerosol Counters," *Adv. Infor. Storage Syst.*, Vol. 5, pp. 387~395.

Hiller, B. and Brown, B., 1992, "Interaction of Individual Alumina Particles with the Head-Disk Interface at Various Velocities," *Adv. Infor. Storage Syst.*, Vol. 5, ASME, pp. 351~361.

Hiller, B. and Singh, G. P., 1994, "Mechanism for Formation of Whiskers on a Flying Magnetic Recording Slider," *IEEE Trans. on Magnetics*, Vol. 30, pp. 1499~1503.

Klaassen, K. B. and van Peppen, J. C. L., 1997, "Electronic Abatement of Thermal Interference in (G)MR Head Output Signals," *IEEE Trans. on Magnetics*. Vol. 33, pp. 2611~2616.

Koka, R., 1989 "Effects of Fine Particles on the Slider Disk Interface in Rigid Disk Drives," *Tribology and Mechanics of Magnetic Storage Systems, STLE publication* SP-26, Vol. 4, pp. 40~46.

McMillan, T. C., Swain, R. C. and Talke, F. E., 1995, "Investigation of Slider Take-off Velocity Using the Acoustic Emission Frequency Spectrum," *IEEE Trans. on Magnetics*, Vol. 31, pp. 2973~2975.

McMillan, T. C. and Talke, F. E., 1998, "Identification of Slider/Disk Contacts Using the Energy of the Acoustic Emission Signal," *IEEE Trans. on Magnetics*, Vol. 34, pp. 1819~1821.

Sawatzky, E., 1998, "Thermal Asperites: MR Heads Face New Dangers," *Data Storage*, Feb. pp. 49~54.

Wang, S., Viswanathan, K. V., Liu, H., "Acoustic Emission of Laser Textured Disks Influenced by Bump Excitation," 1998, *IEEE Trans. on Magnetics*, Vol. 34, pp. 1813~1815.

Zhang, L., Koka, R., Yuen, Y. and Lam, E., 1999, "Particle Induced Damage on Heads and Discs Due to Fine Particles of Different Materials," *IEEE Trans. on Magnetics*, Vol. 35, pp. 927~932.

Zhang, S. and Bogy, D. B., 1997, "Slider Designs for Controlling Contamination," *ASME Journal of Tribology*, Vol. 119, pp. 537~540.